

Supporting information for:

## **Polarization Switching and Light-Enhanced Piezoelectricity in Lead Halide Perovskites**

Mariona Coll<sup>\*1</sup>, Andrés Gomez<sup>1</sup>, Elena Mas-Marzá<sup>2</sup>, Osbel Almora<sup>2</sup>, Germà Garcia-Belmonte<sup>2</sup>, Mariano Campoy-Quiles,<sup>\*1</sup> Juan Bisquert<sup>\*2,3</sup>

<sup>1</sup>Institut de Ciència de Materials de Barcelona (ICMAB-CSIC), Campus UAB, 08193, Bellaterra, Catalonia, Spain

<sup>2</sup>Photovoltaics and Optoelectronic Devices Group, Departament de Física, Universitat Jaume I, 12071, Castelló, Spain

<sup>3</sup>Department of Chemistry, Faculty of Science, King Abdulaziz University, Jeddah, Saudi Arabia

X-ray diffraction  $\theta$ - $2\theta$  scans have been performed in both MAPbI<sub>3</sub> samples, with large and small crystals. Figure 1(a) shows a typical  $\theta$ - $2\theta$  X-ray diffraction patterns of a FTO/TiO<sub>2</sub>/MAPbI<sub>3</sub> sample obtained using a 2D detector. The x axis corresponds to  $2\theta$  and the y axis correspond to  $\chi$ , which varies with constant  $2\theta$ . The Bragg peaks of MAPI and FTO are clearly identified. Note that for both phases, their Bragg reflections appear as rings in the  $\theta$ - $2\theta$  pattern which indicate a random orientation. The integration of the reflection intensities obtained using the 2D- detector lead the spectra presented in figure 1(b). The MAPbI<sub>3</sub> peaks are indexed as a tetragonal phase based on the X-ray diffraction data available in the literature.<sup>1-2</sup> The sample with large crystals shows more intense MAPbI<sub>3</sub> reflections than the sample with small crystals

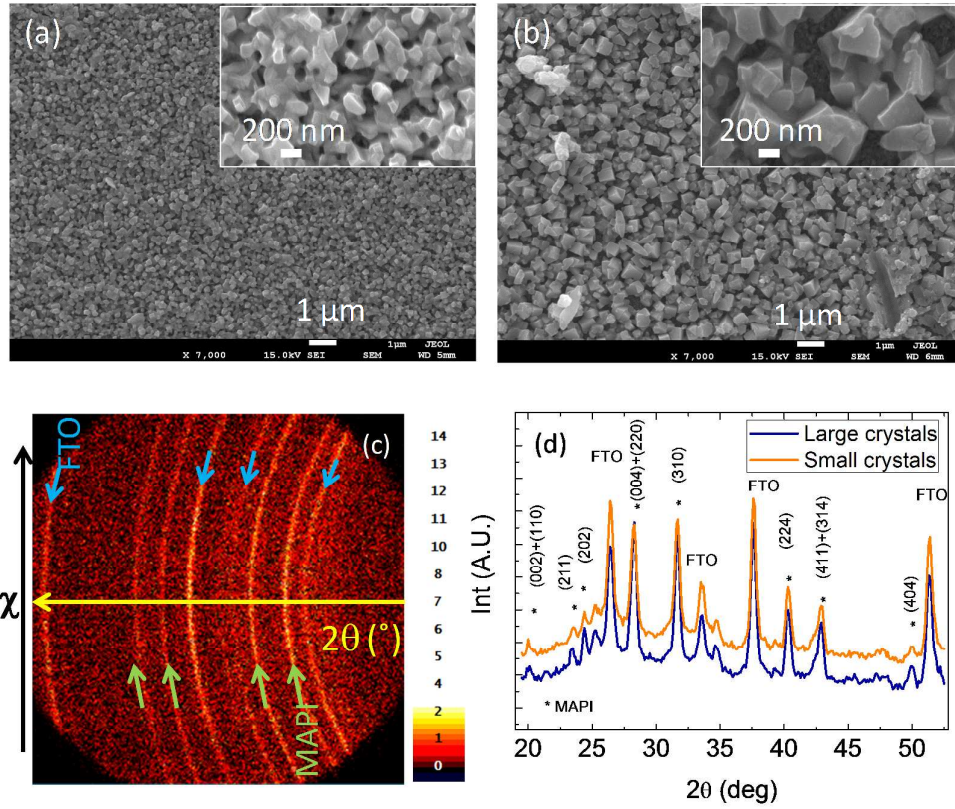


**Figure S1.** SEM study of MAPbI<sub>3</sub> films with (a) small crystals, (b) large crystals. In set shows larger magnification of the main micrograph. (c) X-ray diffraction 2D  $\theta$ -2 $\theta$  scans of typical TiO<sub>2</sub>/FTO/TiO<sub>2</sub>/MAPbI<sub>3</sub> films and (d) Integrated  $\theta$ -2 $\theta$  spectra of a MAPI layer with large crystals (blue) and a MAPI layer with small crystals (orange). MAPbI<sub>3</sub> phase is labeled with an asterisk (\*).

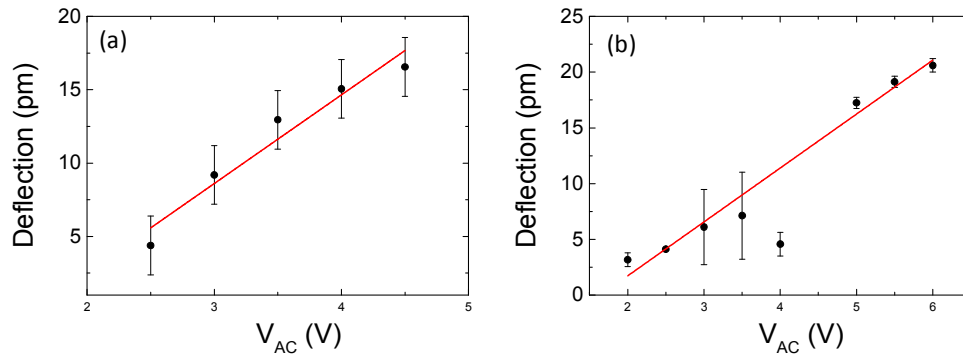


**Figure S2.** Linear dependence between the deflection and the V<sub>AC</sub> for (a) small crystal and (b) large crystals MAPbI<sub>3</sub> films.

To shed light on the existence of the ferroelectric behavior of perovskite halides by means of PFM a small area of the sample was scanned using a DC voltage with the aim to switch the domains to one particular direction (i.e. domains pointing up to the surface) and then scan an inner area using DC voltage with opposite sign to switch the domains  $180^\circ$  (pointing down). This will give important information regarding ferroelectric retention. Typical PFM phase image obtained for BiFeO<sub>3</sub> thin film after switching the ferroelectric domains  $180^\circ$ , is shown in figure S3a,b. We performed this test in our MAPI samples (poling an area of  $4\text{ }\mu\text{m} \times 4\text{ }\mu\text{m}$  with  $-7\text{ V}$  DC bias and then pole back an inner area of  $2\text{ }\mu\text{m} \times \mu\text{m}$  with  $+7\text{ DC}$ ). The PFM-phase image obtained, figure S3(d), is the same as the one obtained when performing a general inspection of the PFM state in a pristine MAPbI<sub>3</sub> film: No evidence of ferroelectric switching was observed. This result contrasts with the ferroelectric switching (hysteresis loops) we previously observed when locally performing switching spectroscopy, figure 3 main manuscript. The main difference between performing a mapping over local switching is the fact that the first experiment takes more than 10 min to be completed and the latter less than 2 seconds. Therefore, it is likely that when performing the mapping, the domain switching is not retained after 10 min.

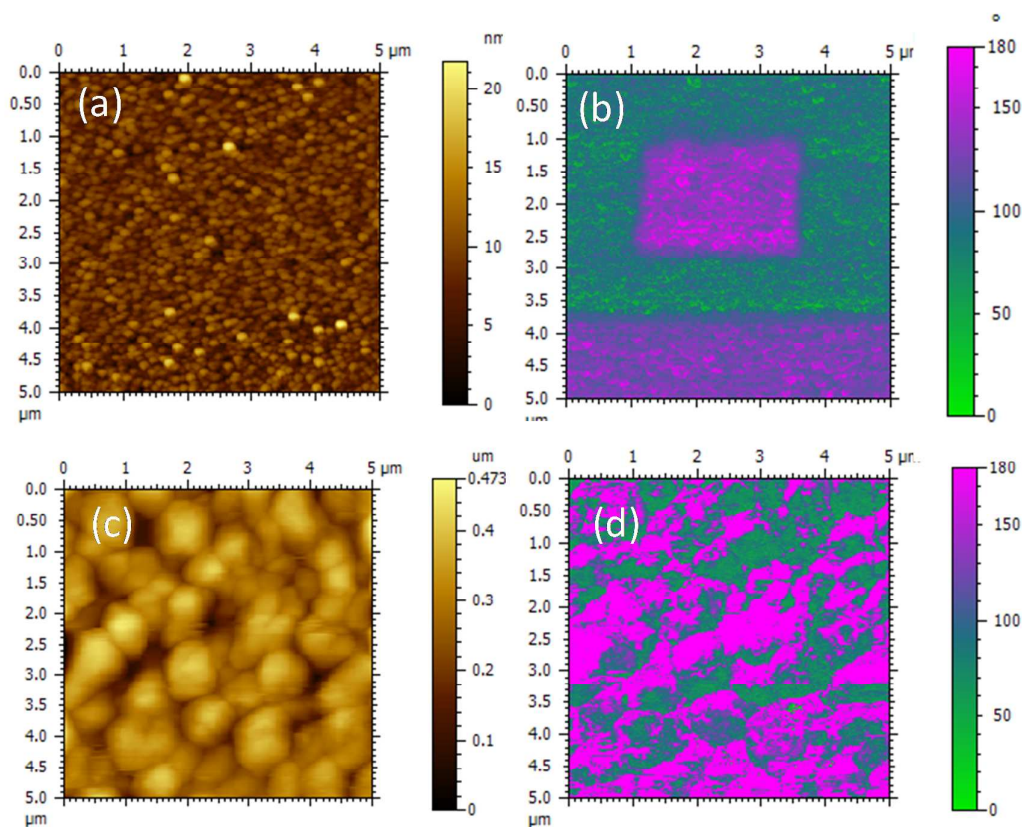


**Figure S3** (a) and (b) 5  $\mu\text{m}$  x 5  $\mu\text{m}$  Topographic and PFM-phase image of a  $\text{BiFeO}_3$  thin film, respectively, after poling two areas with different DC bias.<sup>3</sup> (c) and (d) 5  $\mu\text{m}$  x 5  $\mu\text{m}$  Topographic and PFM-phase image of  $\text{MAPbI}_3$  films after poling two areas with different DC bias.

In order to further investigate the origin of the PFM phase contrast observed in our perovskite halides, we performed PFM measurements on organic/ITO structure used for solar cells where no piezoelectric behavior is expected. The organic film shows an homogeneous and very smooth surface ( $\text{rms}=0.5$  nm), figure S4(a). Importantly, no phase contrast is observed in the piezo-phase image, figure S4(c), which strongly contrasts with the piezo-phase image obtained for the perovskite halide sample, figure S4(d). PFM local spectroscopy was also performed in the organic film in order to locally generate hysteresis loops. The resulting PFM-amplitude and  $-\text{phase}$  loops are shown in figure S4(e)-(g) and they are compared to those previously obtained for the

perovskite halide, figure S4(f)-(h). Note that no square-like and sharp 0-180° hysteresis loops are obtained for the organic film, which agree with the expected non-ferroelectric behavior of these films. Therefore, by comparing the PFM behavior obtained from these two photovoltaic materials it is likely that PFM response obtained in MAPbI<sub>3</sub> films cannot be only due to charge accumulation.

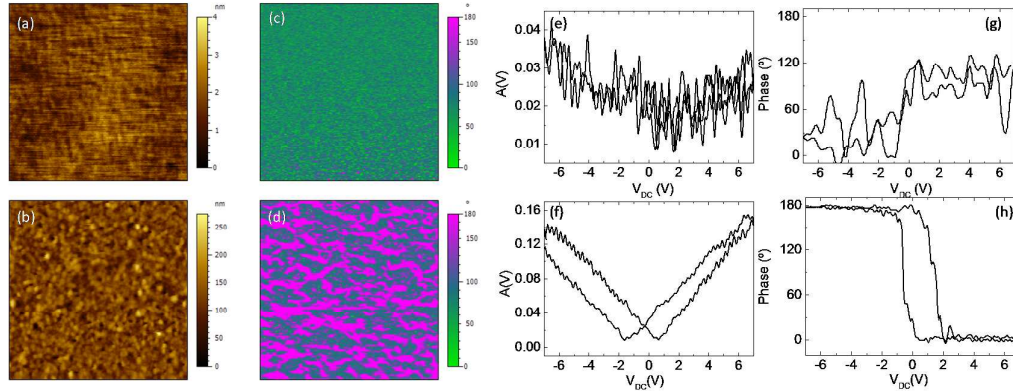


**Figure S4.** PFM analysis of ITO/organic and TiO<sub>2</sub>/FTO/TiO<sub>2</sub>/MAPbI<sub>3</sub> films. (a) and (b) Topographic AFM image acquired simultaneously with the Piezo-phase response (c) and (d) for the organic and MAPbI<sub>3</sub> films, respectively. Piezo-amplitude and piezo-phase hysteresis loops of organic film (e), (g) and MAPI films (f) and (h), respectively.

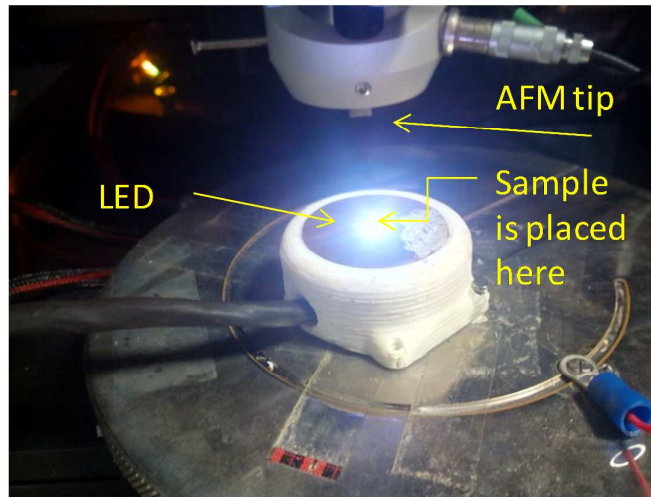


**Figure S5.** Scheme of the PFM setup designed to perform the measurements under illumination.



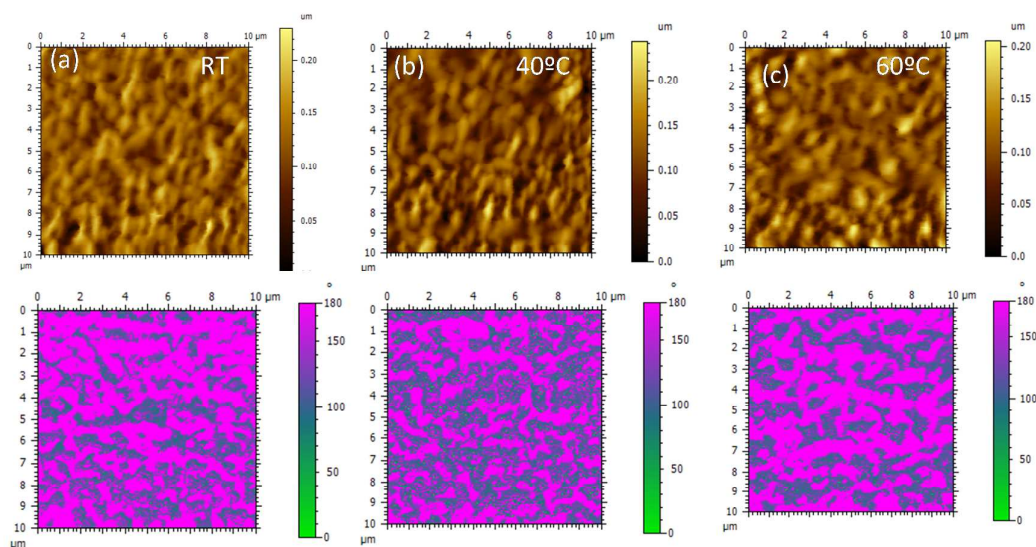


**Figure S6.** AFM topographic and PFM-phase image of MAPbI<sub>3</sub> films acquired under different temperature (a) RT, (b) 40°C, (c) 60°C.

Figure S6 top shows the film morphology of MAPbI<sub>3</sub> films acquired at (a) RT, (b) 40°C and (c) 60°C. Bottom images show their corresponding PFM –phase images.

No changes in the domain features are identified when the sample is exposed to temperatures up to 60°C.

*Solar cell preparation.* For the preparation of the solar cells, a ~300-400 nm-thick of HTM was deposited on top of the perovskite substrates by spin coating at 4000 r.p.m for 30 s under air conditions, using 100 μL of spiro-OMeTAD solution. The spiro-OMeTAD solution was prepared by dissolving 72.3 mg of (2,2',7,7'-tetrakis(N,N'-di-p-methoxyphenylamine)-9,9'-spirobifluorene), 28.8 μL of 4-tert-butylpyridine and 17.5 μL of a stock solution of 520 mg/mL of lithium bis(trifluoromethylsulfonyl)imide in acetonitrile, in 1 mL of chlorobenzene. Subsequently, the deposition of 60 nm of gold was performed by thermal evaporation under ultrahigh vacuum conditions, using a

commercial MBraun vacuum chamber. Before beginning the evaporation the chamber was evacuated until pressure of  $2 \cdot 10^{-6}$  mbar.

*Solar cells characterization.* Current density-voltage ( $J$ - $V$ ) curves were performed under 1 sun illumination ( $100 \text{ mW} \cdot \text{cm}^{-2}$ ) using a xenon arc lamp simulator (Sun 2000, ABET Technologies) with an AM 1.5 G spectral filter and a Keithley 2400, previously calibrated with an NREL-calibrated Si solar cell. All the measurements were performed with an opaque mask of  $0.11 \text{ cm}^2$  and without encapsulation. The electrochemical Impedance spectroscopy measurements were carried out by means of a FRA equipped PGSTAT-30 from Autolab under 1 sun illumination conditions at different applied voltages and applying a 30 mV A/C voltage perturbation over the constant applied bias with a frequency ranging.

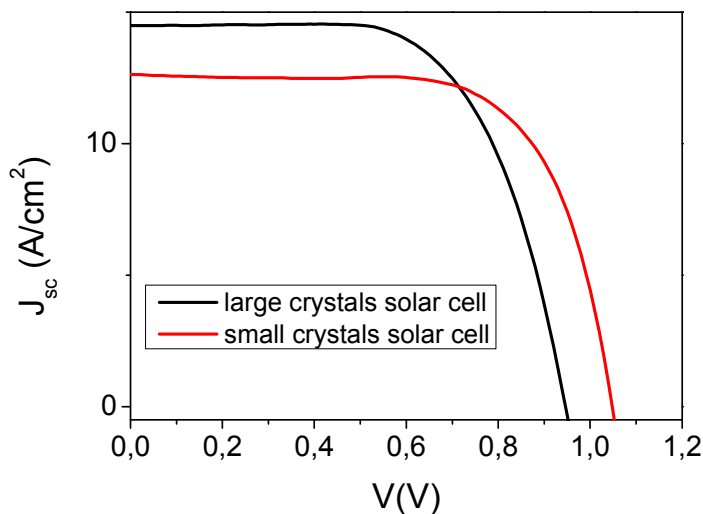


**Figure S7.** J-V curve for solar cells prepared with different crystal size at 1 sun illumination. J-V curves were scanned from positive voltage to zero, at a scan rate of  $50 \text{ mV} \cdot \text{s}^{-1}$

1. Stoumpos, C. C.; Malliakas, C. D.; Kanatzidis, M. G. Semiconducting Tin and Lead Iodide Perovskites with Organic Cations: Phase Transitions, High Mobilities, and Near-Infrared Photoluminescent Properties. *Inorganic Chemistry* **2013**, 52 (15), 9019-9038.
2. Baikie, T.; Fang, Y.; Kadro, J. M.; Schreyer, M.; Wei, F.; Mhaisalkar, S. G.; Graetzel, M.; White, T. J. Synthesis and crystal chemistry of the hybrid perovskite (CH<sub>3</sub>NH<sub>3</sub>)PbI<sub>3</sub> for solid-state sensitised solar cell applications. *Journal of Materials Chemistry A* **2013**, 1 (18), 5628-5641.
3. Coll, M.; Gazquez, J.; Fina, I.; Khayat, Z.; Varela, M.; Alexe, M.; Trolier-McKinstry, S.; Obradors, X.; Puig, T. Nanocrystalline and ferroelectric BiFeO<sub>3</sub> thin films by low temperature atomic layer deposition. submitted.